Reprogramming to recover youthful epigenetic information and restore vision

https://doi.org/10.1038/s41586-020-2975-4

Received: 31 July 2019

Accepted: 22 October 2020

Published online: 2 December 2020

Check for updates

Yuancheng Lu[1], Benedikt Brommer[2,3,11], Xiao Tian[1,11], Anitha Krishnan[3,4,11], Margarita Meer[5,6,11], Chen Wang[2,3], Daniel L. Vera[1], Qiurui Zeng[1], Doudou Yu[1], Michael S. Bonkowski[1], Jae-Hyun Yang[1], Songlin Zhou[2,3], Emma M. Hoffmann[3,4], Margarete M. Karg[3,4], Michael B. Schultz[1], Alice E. Kane[1], Noah Davidsohn[7], Ekaterina Korobkina[3,4], Karolina Chwalek[1], Luis A. Rajman[1], George M. Church[7], Konrad Hochedlinger[8], Vadim N. Gladyshev[5], Steve Horvath[9], Morgan E. Levine[6], Meredith S. Gregory-Ksander[3,4,12], Bruce R. Ksander[3,4,12], Zhigang He[2,3,12] & David A. Sinclair[1,10,12] ✉

Ageing is a degenerative process that leads to tissue dysfunction and death. A proposed cause of ageing is the accumulation of epigenetic noise that disrupts gene expression patterns, leading to decreases in tissue function and regenerative capacity[1–3]. Changes to DNA methylation patterns over time form the basis of ageing clocks[4], but whether older individuals retain the information needed to restore these patterns—and, if so, whether this could improve tissue function—is not known. Over time, the central nervous system (CNS) loses function and regenerative capacity[5–7]. Using the eye as a model CNS tissue, here we show that ectopic expression of *Oct4* (also known as *Pou5f1*), *Sox2* and *Klf4* genes (OSK) in mouse retinal ganglion cells restores youthful DNA methylation patterns and transcriptomes, promotes axon regeneration after injury, and reverses vision loss in a mouse model of glaucoma and in aged mice. The beneficial effects of OSK-induced reprogramming in axon regeneration and vision require the DNA demethylases TET1 and TET2. These data indicate that mammalian tissues retain a record of youthful epigenetic information—encoded in part by DNA methylation—that can be accessed to improve tissue function and promote regeneration in vivo.

The metaphor of the epigenetic landscape, which was first invoked to explain embryonic development[8], is increasingly being seen as relevant to the later stages of life[9]. Evidence from yeast and mammals supports an information theory of ageing[10,11], in which the loss of epigenetic information disrupts youthful gene expression patterns[1–3], leading to cellular dysfunction and senescence[12,13].

DNA methylation patterns are laid down during embryonic development to establish cell type and function. During ageing, for reasons that are currently unclear, these patterns change in ways that can be used to calculate DNA methylation age—a representation of biological age that can predict future health and lifespan[4]. In cell culture, the ectopic expression of the four Yamanaka transcription factors OCT4, SOX2, KLF4 and MYC (OSKM) can reprogram cultured somatic cells to become pluripotent stem cells[14]—a process that erases cellular identity and resets DNA methylation age[4,15]. In a premature-ageing mouse model of Hutchinson–Gilford progeria syndrome, cyclic transgene-mediated expression of the four genes encoding these transcription factors alleviates symptoms and extends lifespan, raising the possibility that OSKM might also counteract normal ageing[16]. The continuous expression of all four factors in mice, however, often induces teratomas[17–19] or is fatal within days[16], ostensibly due to tissue dysplasia[18].

Ageing is generally considered to be a unidirectional process, akin to an increase in entropy. However, living systems are open, not closed, and in some cases biological age can be fully reset, for example in 'immortal' jellyfish and through the cloning of animals by nuclear transfer. Having previously found evidence for epigenetic noise as an underlying cause of ageing[3,13], we wondered whether mammalian cells might retain a faithful copy of epigenetic information from earlier in life that could serve as instructions to reverse ageing[10].

Reset of ageing signatures rather than identity

Our first goal was to find a way to reset the epigenome without erasing cell identity. Among the genes expressing the Yamanaka factors, *Myc*

[1]Department of Genetics, Blavatnik Institute, Paul F. Glenn Center for Biology of Aging Research, Harvard Medical School, Boston, MA, USA. [2]Department of Neurology, Boston Children's Hospital, Harvard Medical School, Boston, MA, USA. [3]Department of Ophthalmology, Harvard Medical School, Boston, MA, USA. [4]Schepens Eye Research Institute of Mass Eye and Ear, Harvard Medical School, Boston, MA, USA. [5]Division of Genetics, Department of Medicine, Brigham and Women's Hospital, Harvard Medical School, Boston, MA, USA. [6]Department of Pathology, Yale School of Medicine, New Haven, CT, USA. [7]Department of Genetics, Wyss Institute for Biologically Inspired Engineering, Harvard University, Boston, MA, USA. [8]Department of Molecular Biology, Cancer Center and Center for Regenerative Medicine, Massachusetts General Hospital, Boston, MA, USA. [9]Department of Human Genetics, David Geffen School of Medicine, University of California Los Angeles, Los Angeles, CA, USA. [10]Laboratory for Ageing Research, Department of Pharmacology, School of Medical Sciences, The University of New South Wales, Sydney, New South Wales, Australia. [11]These authors contributed equally: Benedikt Brommer, Xiao Tian, Anitha Krishnan, Margarita Meer. [12]These authors jointly supervised this work: Meredith S. Gregory-Ksander, Bruce R. Ksander, Zhigang He, David A. Sinclair. ✉e-mail: david_sinclair@hms.harvard.edu

is an oncogene that reduces the lifespan of mice[20] and is not required for the initiation of cellular reprogramming[21]. We therefore excluded MYC from our experiments and expressed only the transcription factors OCT4, SOX2 and KLF4 (OSK) in fibroblasts from old mice, after which we monitored the effect on genes that are known to be altered with age, including *Lmnb1*, *Chaf1b*, and those from the H2a and H2b families[13]. Even without MYC, the expression of OSK for five days promoted a youthful mRNA profile, with no apparent loss of cellular identity or induction of NANOG—a transcription factor that is indicative of pluripotency and oncogenicity (Extended Data Fig. 1a–c).

Next we tested the long-term safety of ectopically expressing OSK in vivo. To deliver and control OSK expression in mice, we engineered a dual adeno-associated virus (AAV) system under the tight control of a tetracycline response element (TRE) promoter (Fig. 1a). The TRE promoter can be activated either by reverse tetracycline-controlled transactivator (rtTA) in the presence of the tetracycline derivative doxycycline (DOX) ('Tet-On') or by tetracycline-controlled transactivator (tTA) in the absence of DOX ('Tet-Off'). Extraneous AAV sequences were removed from the vector to accommodate OSK as a polycistron. To test if AAV-mediated OSK expression was toxic in vivo, we co-infected young (5-month-old) and aged (20-month-old) mice with AAV9-rtTA;TRE-OSK via intravenous delivery. OSK expression was then induced by providing DOX in the drinking water, our rationale being that the weak tropism of AAV for the digestive system might avoid the dysplasia and weight loss that is seen in transgenic mouse models[18] (Extended Data Fig. 1d–i). After 10–18 months of continuous OSK induction, no increase in tumour incidence or negative effects on overall health were observed, indicating that cellular identity was maintained in OSK-expressing cells (Extended Data Fig. 1j–n).

OSK stimulates axon regeneration

Almost all species experience a decline in regenerative potential during ageing. In mammals, one of the first systems to lose regenerative potential is the CNS[5–7]. Retinal ganglion cells (RGCs) of the CNS project axons away from the retina to form the optic nerve. If damaged, RGCs of embryos and neonates can regenerate axons, but this capacity is lost within days after birth, probably due to a molecular program that is intrinsic to the RGCs[6,22]. Attempts to reverse optic-nerve damage have been only moderately successful, and there are currently no treatments that can restore eyesight either in late-stage glaucoma or in old age[23].

To test whether it is possible to provide adult RGCs with the regenerative capacity of younger RGCs, we induced OSK in an optic-nerve crush-injury model. To deliver genes into the retina, Tet-Off AAV2s carrying an OSK polycistron were injected into the vitreous body, resulting in DOX-responsive OSK gene expression in around 40% of RGCs, as estimated by immunostaining (Fig. 1b, Extended Data Fig. 2a, b). Even after 15 months of continuous induction, OSK expression did not induce any tumours or structural changes in the retina (Extended Data Fig. 2c–i, Supplementary Videos 1–3).

In a separate cohort, RGCs were infected with Tet-Off AAV2 and optic-nerve crush was performed two weeks later (Fig. 1c). After another two weeks, Alexa Fluor 555-conjugated cholera toxin subunit B (CTB)—an anterograde axonal tracer—was delivered by intravitreal injection to quantify axon regeneration. Independent of RGC proliferation (Extended Data Fig. 3a, b), the greatest extent of axon regeneration and RGC survival occurred when all three genes were delivered and expressed as a polycistron within the same AAV particle (Fig. 1d, e). Notably, when polycistronic OSK was induced for 12–16 weeks, regenerating and sprouting RGC axon fibres extended over 5 mm into the chiasm, where the optic nerve connects to the brain (Extended Data Fig. 3c, d). Suppression of polycistronic OSK by DOX treatment prevented both regenerative and survival effects (Fig. 1d, e, Extended Data Fig. 3e).

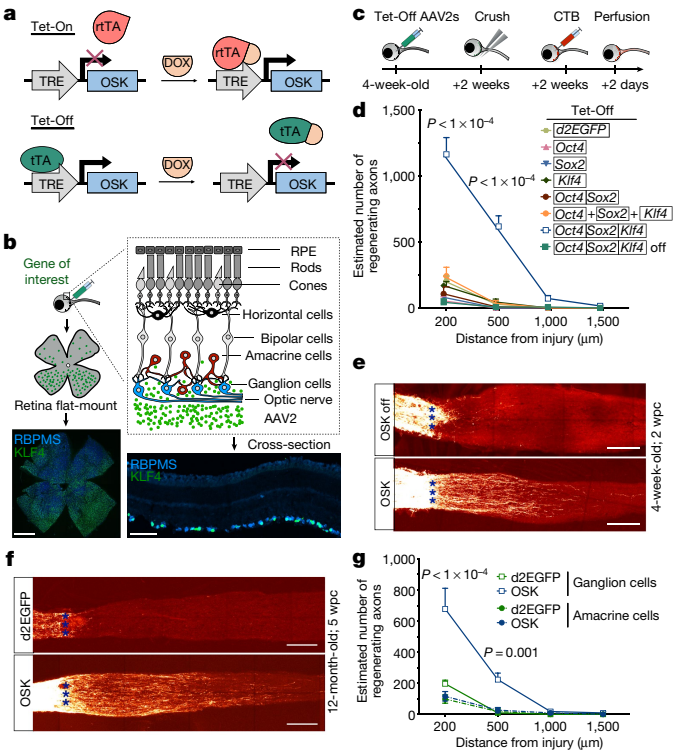

Fig. 1 | AAV2-delivered polycistronic OSK promotes axon regeneration and RGC survival after optic nerve injury. a, Schematic of the Tet-On and Tet-Off dual AAV vectors. OSK denotes *Oct4*-P2A-*Sox2*-T2A-*Klf4*. **b**, Schematic (top) and representative retinal wholemount (bottom left) and cross-sections (bottom right) ($n = 10$), two weeks after intravitreal injection of AAV2-tTA;TRE-OSK, showing *Klf4* (green) expression in the RGCs (blue, visualized by RBPMS as marker). Scale bars, 1 mm (left); 100 μm (right). **c**, Experimental outline of the optic-nerve crush-injury study using the Tet-Off system. 555-CTB was used for anterograde axonal tracing. **d**, The number of axons 16 days after crush injury, at distances distal to the lesion, in mice treated with AAV2 encoding: destabilized enhanced green fluorescent protein (d2EGFP); *Oct4*; *Sox2*; *Klf4*; *Oct4* and *Sox2*; all three OSK genes on three monocistronic AAV2s (indicated as separated by + signs); or all three OSK genes on a single polycistronic AAV2 ($n = 5, 4, 4, 4, 4, 4$ and 7 eyes, respectively). In **d**, **e**, suppression of polycistronic OSK expression by DOX ($n = 5$ eyes) is shown as OSK off. **e**, Representative images of longitudinal sections through the optic nerves of 4-week-old (young) mice after receiving intravitreal injections of AAV2-tTA;TRE-OSK in the presence ($n = 5$) or absence ($n = 7$) of DOX. CTB-labelled axons are shown 16 days post-crush. Asterisks indicate the optic-nerve crush site. **f**, Representative confocal images of longitudinal sections through the optic nerve showing CTB-labelled axons in 12-month-old (old) mice, 5 weeks post-crush, with AAV2-mediated expression of either GFP or OSK. Representative results from $n = 5$ eyes. Scale bars (**e**, **f**), 200 μm. **g**, The number of axons 16 days post-crush at multiple distances distal to the lesion site in transgenic Cre lines that selectively express OSK either in RGCs (Vglut2-Cre) or in amacrine cells (Vgat-Cre) after intravitreal injection of AAV2-FLEx-tTA;TRE-OSK ($n = 4$ eyes for each condition). Further details are given in Extended Data Fig. 4e–h. One-way ANOVA with Bonferroni correction (**d**, **g**), with comparisons to d2EGFP shown in **f**. All data are presented as mean ± s.e.m.

When *Oct4*, *Sox2* and *Klf4* were co-delivered by separate monocistronic AAVs, no effect on axon regeneration was observed; this was ostensibly due to the lower frequency of co-infection or inconsistent stoichiometry (Fig. 1d, Extended Data Fig. 3f–i). When delivered singly, *Oct4* or *Sox2* alone increased RGC survival slightly (Extended Data Fig. 3e), but none of the single factors alone had any effect on regenerative capacity (Fig. 1d). Because *Klf4* can repress rather than promote axonal growth[24], we tested a dual-cistron of only *Oct4* and *Sox2* and observed no regenerative effect.

Many regenerative approaches that work well in young individuals often fail in older ones[25,26]. In 12-month-old mice, OSK treatment doubled RGC survival, similar to the results observed in 1- and 3-month-old mice (Extended Data Fig. 4a). Although axon regeneration was slightly weaker in the older mice (Extended Data Fig. 4b), when treatment was extended for 3 more weeks (thus measuring regeneration 5 weeks after the optic-nerve crush), robust axon regeneration still occurred, with no increase in RGC number (Fig. 1f, Extended Data Fig. 4c, d). These data indicate that ageing does not greatly diminish the ability of OSK transcription factors to induce axon regeneration.

To test whether OSK was acting directly on RGCs or through amacrine cells[27]—the other type of retinal cells that AAV2 can infect after intravitreal injection—we introduced tTA in a double-floxed inverse orientation (AAV2-FLEx-tTA) with AAV2-TRE-OSK into two Cre transgenic mouse lines, so that OSK was selectively expressed either in RGCs (Vglut2-Cre) or amacrine cells (Vgat-Cre) (Extended Data Fig. 4e, f). OSK expression in RGCs alone promoted axon regeneration, whereas expression in amacrine cells did not (Fig. 1g, Extended Data Fig. 4g, h). The survival frequency of OSK-positive RGCs was roughly three times that of nearby OSK-negative cells or that of RGCs in GFP-expressing retinas, resulting in a greater relative abundance of OSK-positive RGCs after injury (Extended Data Fig. 4i–k). Therefore, the ability of OSK to increase survival seems to be mediated within the RGC and is largely cell-autonomous. The mRNA levels of *Stat3*, a pro-regeneration gene[28], robustly increased in response to OSK and were maintained post-injury (Extended Data Fig. 5a, Supplementary Table 1). *Stat3* upregulation, however, does not seem to be mediated by the PTEN–mTOR–S6K or the SOCS3 pathways, two canonical *Stat3* regulatory pathways that affect RGC axon regeneration[29,30] (Extended Data Fig. 5b, c, Supplementary Table 1).

OSK counters injury-induced DNA methylation ageing

Currently, there is no known treatment that can induce robust RGC axon regeneration when the treatment is started after crush injury. Using our Tet-On AAV system, which rapidly induces OSK expression (Fig. 2a, Extended Data Figs. 2b, 5d, e), we observed significant improvement in axon regeneration and RGC survival, even when OSK was induced after injury. The longer the duration of the OSK induction the greater the distance the axons extended, with no sign of RGC proliferation (Fig. 2b, c, Extended Data Fig. 5f).

Given the effectiveness of OSK induction after injury and the ability of Yamanaka factors to reverse DNA methylation age in vitro[4,15,31,32], we speculated that OSK might act to regenerate axons by counteracting the effect of injury on DNA methylation. The DNA methylation age of RGCs was calculated on the basis of a ribosomal DNA methylation clock[33], which provided the best site coverage (67 out of 72 CpG sites) and was highly correlated with chronological age (Extended Data Fig. 5g). At day 4 after injury, RGCs experienced an acceleration of DNA methylation age, whereas OSK expression counteracted this effect (Fig. 2d). Patterns of global DNA methylation were also altered by injury in a manner similar to that of ageing, without affecting average DNA methylation levels (Extended Data Fig. 5h, i). Notably, OSK reversed the global DNA methylation changes caused by injury, and this reversal was enriched at genes that are associated with light detection and synaptic transmission (Fig. 2e, Extended Data Fig. 5j, k).

Regeneration requires DNA demethylation

Next we asked whether the DNA methylation changes induced by OSK are necessary for RGC survival and axon regrowth. DNA demethylation is catalysed by ten-eleven translocation methylcytosine dioxygenases (TET1–TET3), either passively through DNA replication or actively—even in non-replicating cells—by reversion to cytosine via thymine DNA glycosylase (TDG)[34]. Because TET1 and TET2—but not TET3—were

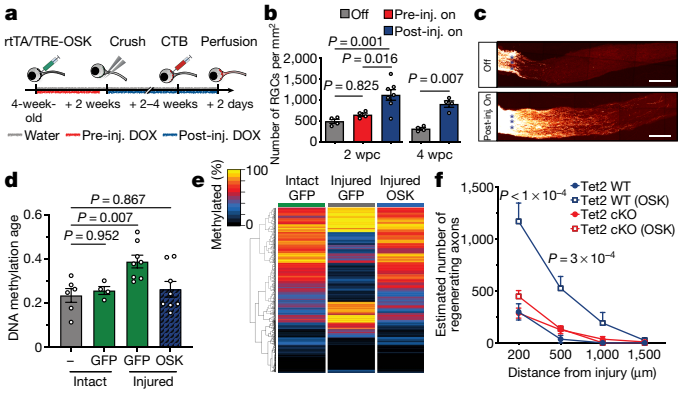

Fig. 2 | DNA demethylation is required for OSK-induced axon regeneration after injury. a, Strategies for induction of OSK pre- and post-injury. **b**, Survival of RGCs (number of RGCs per mm^2) at 2 and 4 weeks post-crush (wpc) in response to OSK induction either pre- or post-injury (inj.) ($n = 4$ eyes, except for the post-injury 'on' group at 2 weeks post-crush, for which $n = 7$ eyes). **c**, Representative longitudinal sections through the optic nerve showing CTB-labelled axons at 4 weeks post-crush, without (top) or with (bottom) the induction of OSK after injury. Asterisks indicate the optic-nerve crush site. Results are representative from $n = 4$ eyes. Scale bars, 200 μm. **d**, Ribosomal DNA methylation age (in months) of 6-week-old RGCs isolated from axon-intact retinas infected with or without GFP-expressing AAV2 (intact), or from axon-injured retinas infected with GFP- or OSK-expressing AAV2 at 4 days post-crush (injured) ($n = 6$, 4, 8 and 8 eyes, respectively). DNA methylation age estimates of neurons tend to be lower than their chronological ages but remain correlated (see Extended Data Fig. 5g and Methods). **e**, Hierarchical clustered heat map of DNA methylation levels of CpGs that significantly changed in RGCs after crush injury (intact GFP vs injured GFP, $q < 0.05$) and the effect of OSK at 4 days post-crush (injured OSK). **f**, Axon regeneration in response to OSK expression (AAV2-tTA; TRE-OSK), 16 days post-crush in *Tet2*$^{flox/flox}$ mice infected with saline (Tet2 wild type (WT); $n = 3$ for each condition) or AAV2-Cre (Tet2 cKO; $n = 4$ for each condition). One-way ANOVA with Bonferroni's multiple comparison test (**b**, **d**, **f**). For all bar graphs, data are mean ± s.e.m.

upregulated by OSK[35,36] (Extended Data Fig. 6a), we tested the effect of knocking down their encoding genes *Tet1* or *Tet2* (using short hairpin (sh)RNA delivered by AAV[37]) in the context of damaged, OSK-treated RGCs (Extended Data Fig. 6b–d).

The knockdown of either *Tet1* or *Tet2* blocked the ability of OSK to increase *Stat3* mRNA levels and to promote RGC survival and axon regeneration (Extended Data Fig. 6e–g). Knocking out *Tet2* in RGCs by delivering AAV2-Cre[30] intravitreally to *Tet2*$^{flox/flox}$ mice also abrogated the increase in regeneration and survival (Fig. 2f, Extended Data Fig. 6h–j). OSK-expressing RGCs showed no evidence of DNA replication in a 5-bromo-2′-deoxyuridine (BrdU) assay (Extended Data Fig. 3a, b), and knockdown of *Tdg*[38] completely abolished the beneficial effects of OSK (Extended Data Fig. 7a–d); however, a global reduction of DNA methylation mediated by overexpression of the TET1 catalytic domain[39] had no protective or regenerative effect (Extended Data Fig. 7e–h). These data indicate that active DNA demethylation is necessary—but is not sufficient by itself—in order for OSK to protect RGCs and to regenerate axons (Extended Data Fig. 7i).

Axon regeneration in human neurons

Paralleling the mouse RGC data, the expression of OSK in differentiated human neurons effectively counteracted axonal loss and the advancement of DNA methylation age induced by vincristine—a chemotherapeutic drug that induces axon injury—in the absence of cell proliferation or global DNA demethylation (Extended Data Fig. 8a–g). Nine days after damage, the neurite area was 15-fold greater in the rejuvenated OSK-transduced cells compared with control cells (Extended Data Fig. 8h, i).

OSK-mediated recovery of the neurite area, as well as both the number and the length of axons, were blocked by *Tet2* knockdown but not by inhibition of the mTOR–S6K pathway (Extended Data Fig. 8j–s). Again, overexpression of the TET1 catalytic domain alone failed to promote axon regeneration (Extended Data Fig. 8t). The ability of OSK to reprogram neurons and to promote axon growth in a *Tet2*-dependent manner therefore seems to be conserved across mice and humans.

Recovery of vision in mice with glaucoma

We then tested whether OSK induction could restore the function of RGCs in a disease setting. Glaucoma, a leading cause of age-related blindness worldwide, is characterized by a progressive loss of RGCs and their axons, and often coincides with increased intraocular pressure. We induced increased intraocular pressure unilaterally for 21 days by injecting microbeads into the anterior chamber of the eye[40] (Fig. 3a, b), using saline injections as non-glaucomatous controls. At the 4-week time point, after a significant decrease in axonal density and the number of RGCs (baseline, Extended Data Fig. 9a, b), AAVs were injected intravitreally and OSK expression was induced for another 4 weeks (Fig. 3a). Compared with glaucomatous eyes that received either PBS or AAVs with no OSK induction (−OSK), the OSK-treated glaucomatous eyes (+OSK) presented with a restored axon density equivalent to that in the non-glaucomatous eyes, with no evidence of RGC proliferation (Extended Data Fig. 9c, d).

A significant increase in visual acuity relative to the pre-treatment function baseline was observed for eyes treated with OSK: the optomotor response assay indicated that half of the visual acuity lost from increased intraocular pressure was restored (Fig. 3c, d). A similar improvement associated with OSK expression was also seen in pattern electroretinogram (PERG) analysis (N1+P1), a readout of electrical waves generated specifically by RGCs (Fig. 3e, f). To our knowledge, this is the first example of vision-loss reversal after glaucomatous injury has occurred; previous attempts have focused on neuroprotection delivered at an early stage to prevent further disease progression[41,42] (Supplementary Information).

Restoration of vision in old mice

The finding that OSK induction could effectively restore the DNA methylation age of RGCs after injury indicated that vision loss caused by natural ageing might be reversible too. To test this, we treated 3- and 11-month-old mice with OSK AAVs and induced OSK expression for 4 weeks (Fig. 4a). Optomotor response and PERG measurements were then carried out. In the absence of OSK induction, there was a significant reduction in visual acuity and in RGC electrical activity by 12 months of age—a loss that was restored by OSK induction (Fig. 4b, Extended Data Fig. 9e). Restoration of visual acuity was not seen in 18-month-old mice (Extended Data Fig. 9e, f), probably because assessment was hindered by an age-dependent increase in corneal opacity[43].

Because there was no obvious increase in the number of RGCs or in axon density in the 12-month-old mice treated with +OSK AAV (Extended Data Fig. 9g, h), we hypothesized that the visual improvements were due to transcriptomic changes. RGCs from 12-month-old mice, either untreated or treated with AAVs for 4 weeks, were purified by fluorescence-activated cell sorting and analysed by RNA sequencing. Compared with RGCs from young (5-month-old) mice, the mRNA levels of 464 genes were altered during ageing. Around 90% of these were restored to youthful levels by OSK treatment (Fig. 4c, d, Extended Data Fig. 9i, Supplementary Table 2). Of the 268 age-downregulated genes, 44 are linked to sensory perception and axon targeting[44], raising the possibility that they contribute to the decline in vision caused by ageing (Fig. 4d, Extended Data Figs. 9j, 10a). Another 196 genes that were upregulated during ageing are involved in ion transport or neuronal projection development, including *Efemp1* (Extended Data Fig. 10b–d), a TET1- and TET2-regulated gene that is associated with glaucoma[45] and age-related macular degeneration[46].

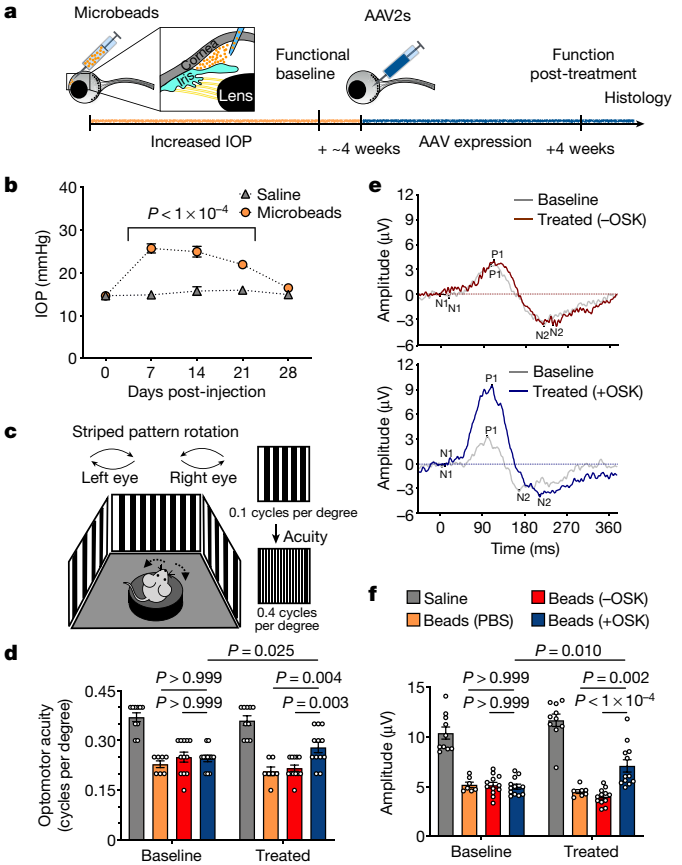

Fig. 3 | Four weeks of OSK expression reverses vision loss after glaucomatous damage has already occurred. a, Experimental outline of the induced glaucoma studies using 8-week-old mice. **b**, Intraocular pressure (IOP) measured weekly by rebound tonometry for the first 4 weeks after the injection of microbeads ($n = 29$ mice) or saline ($n = 10$ mice). **c**, High-contrast visual stimulation to measure optomotor response. Reflexive head movements were tracked in response to the rotation of a moving striped pattern that increased in spatial frequency. **d**, Optomotor response of each mouse before treatment (baseline) and 4 weeks after intravitreal injection of AAVs (treated; see **f** for key) ($n = 10, 7, 12$ and 12 mice for each condition; similar results from 3 independent experiments combined). **e**, Representative PERG waveforms in response to a reversing contrast checkerboard pattern, recorded from the same eye both at the pre-injection baseline and at 4 weeks after −OSK (top) or +OSK (bottom) AAV injection. **f**, Mean PERG amplitudes of recordings from each mouse in **d** at the baseline before treatment and at 4 weeks after intravitreal AAV injection ($n = 10, 7, 12$ and 12 mice for each condition; similar results from 3 independent experiments combined). −OSK (not induced), AAV2-rtTA;TRE-OSK; +OSK (induced), AAV2-tTA;TRE-OSK. For **b**, a two-way ANOVA with Bonferroni correction between groups was used; for **d**, **f**, a two-way mixed ANOVA with Bonferroni correction between groups was used for the overall effect of time and treatment, and before and after treatments were analysed using a paired two-tailed Student's *t*-test. Data in **b**, **d** and **f** are presented as mean ± s.e.m.

To gain insights into how DNA methylation changes might be involved in the effects of OSK, we used machine learning to identify a methylation ageing signature based on 1,226 sites from genome-wide DNA methylation datasets, derived from the first principal component (PC1) in multi-age training samples (Extended Data Fig. 10e, Supplementary Table 3). In an independent set of test samples, OSK reversed the DNA methylation ageing signature in the context of both injury and ageing (Fig. 4e, Extended Data Fig. 10f). Notably, the signature CpG sites were associated with genes that are involved in synaptic and neuronal processes and are enriched for the binding of polycomb repressive complex

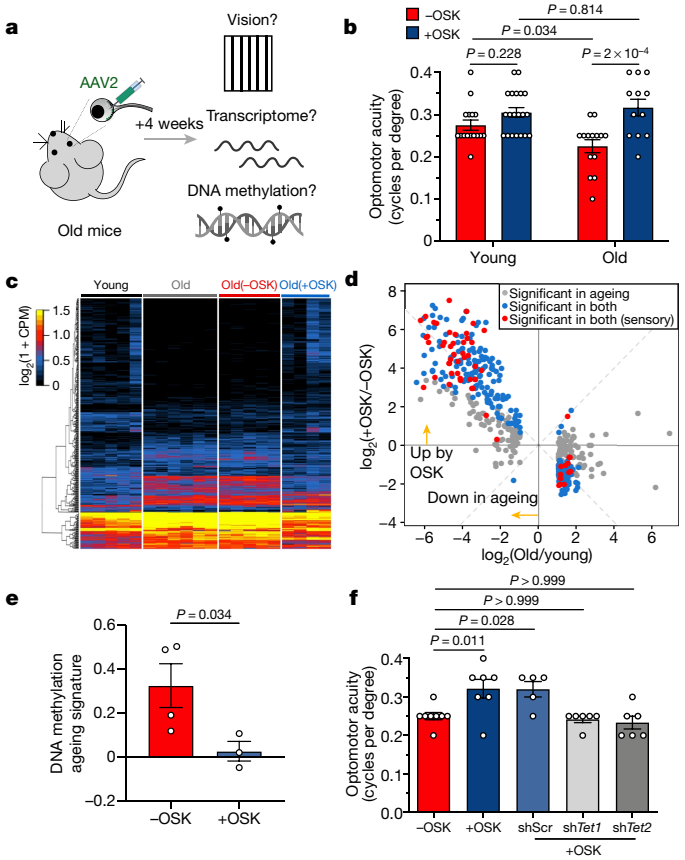

Fig. 4 | Restoration of youthful vision, transcriptome and DNA methylation ageing signature in old mice. a, Experimental outline for testing the effect of reprogramming in old mice. **b**, Visual acuity in young (4-month-old) and old (12-month-old) mice after 4 weeks of −OSK or +OSK treatment ($n = 16, 20, 14$ and 12 eyes, respectively; similar results from 2 independent experiments combined). **c**, **d**, Hierarchical clustered heat map (**c**) and scatter plot (**d**) showing mRNA levels of 464 genes that were differentially expressed between young and old RGCs and the effect of OSK. RGCs were sorted from the retinas of untreated young (5-month-old, $n = 5$), old (12-month-old, $n = 6$) or treated old (12-month-old; −OSK, $n = 5$; +OSK, $n = 4$) mice. The gene selection criteria for **c**, **d** are described in Methods. **e**, DNA methylation ageing signatures of RGCs from 12-month-old mice infected for 4 weeks with −OSK or +OSK ($n = 4$ and 3 retinas). **f**, Visual acuity in old (12-month-old) mice treated for 4 weeks with −OSK, +OSK, or +OSK together with short hairpin scramble RNA (shScr), shTet1 or shTet2 ($n = 8, 7, 5, 6$ and 6 eyes, respectively). −OSK: AAV2-rtTA;TRE-OSK (**b**); AAV2-TRE-OSK (**c**, **d**); AAV2-tTA;TRE-d2EGFP (**e**); +OSK: AAV2-tTA;TRE-OSK (**b**–**f**). Two-way ANOVA with Bonferroni correction (**b**); Kruskal–Wallis test (**e**); one-way ANOVA with Bonferroni correction, with comparisons to the −OSK group (**f**). For all bar graphs, data are mean ± s.e.m.

2 (PRC2) and its histone methyltransferase product—trimethylated Lys27 of histone H3 (H3K27me3)—both of which are known to recruit TET enzymes[47,48] (Extended Data Fig. 10g–i). Knockdown of either *Tet1* or *Tet2* altered the methylation status of the signature CpG sites in a similar manner and counteracted the effect of OSK on DNA methylation age (Extended Data Fig. 10j–l). Both *Tet1* and *Tet2* were also required for the improvement of RGC function and vision in 12-month-old mice (Fig. 4f, Extended Data Fig. 10m), indicating that changes in DNA methylation might have a functional role in the restoration of vision in old mice by OSK.

Discussion

Here we show that it is possible to safely reverse the age of a complex tissue and restore its biological function in vivo. Using the eye as a model system, we present evidence that the ectopic expression of OSK transcription factors safely induces in vivo epigenetic restoration of aged CNS neurons, without causing a loss of cell identity or pluripotency. Instead, OSK promotes a youthful epigenetic signature and gene-expression pattern that causes the neurons to function as though they were young again. The requirement for active demethylation in this process supports the idea that changes in DNA methylation patterns are involved in the ageing process and its functional reversal (Extended Data Fig. 10n). However, we do not wish to imply that DNA methylation is the only epigenetic mark involved in this process. It is likely to involve other transcription factors and epigenetic modifications, such as the PRC2 complex and H3K27me3, both of which are involved in maintaining stem cell plasticity and are associated with DNA methylation clock sites[4,49,50].

Perhaps the most interesting question raised by these data is how cells encode and store youthful epigenetic information. Possibilities for information storage include covalent DNA modifications, DNA-binding proteins, RNA-guided chromatin modifying factors, and RNA–DNA hybrids that are established early in life. The role of these youth marks would be akin to the 'observer' in information theory, which preserves an original backup copy of information in case it is lost or obscured by noise[11]. We suggest that epigenetic reprogramming, either by gene therapy or other means, could promote tissue repair and the reversal of age-related decline in humans.

Online content

Any methods, additional references, Nature Research reporting summaries, source data, extended data, supplementary information, acknowledgements, peer review information; details of author contributions and competing interests; and statements of data and code availability are available at https://doi.org/10.1038/s41586-020-2975-4.

1. Sinclair, D. A., Mills, K. & Guarente, L. Accelerated aging and nucleolar fragmentation in yeast sgs1 mutants. *Science* **277**, 1313–1316 (1997).
2. Imai, S. & Kitano, H. Heterochromatin islands and their dynamic reorganization: a hypothesis for three distinctive features of cellular aging. *Exp. Gerontol.* **33**, 555–570 (1998).
3. Oberdoerffer, P. et al. SIRT1 redistribution on chromatin promotes genomic stability but alters gene expression during aging. *Cell* **135**, 907–918 (2008).
4. Horvath, S. DNA methylation age of human tissues and cell types. *Genome Biol.* **14**, 3156 (2013).
5. Kennard, M. A. Relation of age to motor impairment in man and in subhuman primates. *Arch. Neurol. Psychiatry* **44**, 377–397 (1940).
6. Goldberg, J. L., Klassen, M. P., Hua, Y. & Barres, B. A. Amacrine-signaled loss of intrinsic axon growth ability by retinal ganglion cells. *Science* **296**, 1860–1864 (2002).
7. Yun, M. H. Changes in regenerative capacity through lifespan. *Int. J. Mol. Sci.* **16**, 25392–25432 (2015).
8. Waddington, C. H. & Kacser, H. *The Strategy of the Genes: a Discussion of Some Aspects of Theoretical Biology* (Allen & Unwin, 1957).
9. Sen, P., Shah, P. P., Nativio, R. & Berger, S. L. Epigenetic mechanisms of longevity and aging. *Cell* **166**, 822–839 (2016).
10. Sinclair, D. A. & LaPlante, M. D. *Lifespan: Why We Age—and Why We Don't Have To* 13–23, 158–175 (Simon & Schuster, 2019).
11. Shannon, C. E. A mathematical theory of communication. *Bell Syst. Tech. J.* **27**, 379–423 (1948).
12. López-Otín, C., Blasco, M. A., Partridge, L., Serrano, M. & Kroemer, G. The hallmarks of aging. *Cell* **153**, 1194–1217 (2013).
13. Yang, J.-H. et al. Erosion of the epigenetic landscape and loss of cellular identity as a cause of aging in mammals. Preprint at https://doi.org/10.1101/808642 (2019).
14. Takahashi, K. & Yamanaka, S. Induction of pluripotent stem cells from mouse embryonic and adult fibroblast cultures by defined factors. *Cell* **126**, 663–676 (2006).
15. Petkovich, D. A. et al. Using DNA methylation profiling to evaluate biological age and longevity interventions. *Cell Metab.* **25**, 954–960.e6 (2017).
16. Ocampo, A. et al. In vivo amelioration of age-associated hallmarks by partial reprogramming. *Cell* **167**, 1719–1733.e12 (2016).
17. Ohnishi, K. et al. Premature termination of reprogramming in vivo leads to cancer development through altered epigenetic regulation. *Cell* **156**, 663–677 (2014).
18. Abad, M. et al. Reprogramming in vivo produces teratomas and iPS cells with totipotency features. *Nature* **502**, 340–345 (2013).
19. Senís, E. et al. AAV vector-mediated in vivo reprogramming into pluripotency. *Nat. Commun.* **9**, 2651 (2018).
20. Hofmann, J. W. et al. Reduced expression of MYC increases longevity and enhances healthspan. *Cell* **160**, 477–488 (2015).

21. Rand, T. A. et al. MYC releases early reprogrammed human cells from proliferation pause via retinoblastoma protein inhibition. *Cell Rep*. **23**, 361–375 (2018).
22. Laha, B., Stafford, B. K. & Huberman, A. D. Regenerating optic pathways from the eye to the brain. *Science* **356**, 1031–1034 (2017).
23. Roska, B. & Sahel, J. A. Restoring vision. *Nature* **557**, 359–367 (2018).
24. Moore, D. L. et al. KLF family members regulate intrinsic axon regeneration ability. *Science* **326**, 298–301 (2009).
25. Geoffroy, C. G., Hilton, B. J., Tetzlaff, W. & Zheng, B. Evidence for an age-dependent decline in axon regeneration in the adult mammalian central nervous system. *Cell Rep*. **15**, 238–246 (2016).
26. Yao, K. et al. Restoration of vision after de novo genesis of rod photoreceptors in mammalian retinas. *Nature* **560**, 484–488 (2018).
27. Zhang, Y. et al. Elevating growth factor responsiveness and axon regeneration by modulating presynaptic inputs. *Neuron* **103**, 39–51.e5 (2019).
28. Luo, X. et al. Enhanced transcriptional activity and mitochondrial localization of STAT3 co-induce axon regrowth in the adult central nervous system. *Cell Rep*. **15**, 398–410 (2016).
29. Park, K. K. et al. Promoting axon regeneration in the adult CNS by modulation of the PTEN/mTOR pathway. *Science* **322**, 963–966 (2008).
30. Sun, F. et al. Sustained axon regeneration induced by co-deletion of PTEN and SOCS3. *Nature* **480**, 372–375 (2011).
31. Olova, N., Simpson, D. J., Marioni, R. E. & Chandra, T. Partial reprogramming induces a steady decline in epigenetic age before loss of somatic identity. *Aging Cell* **18**, e12877 (2019).
32. Sarkar, T. J. et al. Transient non-integrative expression of nuclear reprogramming factors promotes multifaceted amelioration of aging in human cells. *Nat. Commun*. **11**, 1545 (2020).
33. Wang, M. & Lemos, B. Ribosomal DNA harbors an evolutionarily conserved clock of biological aging. *Genome Res*. **29**, 325–333 (2019).
34. Wu, X. & Zhang, Y. TET-mediated active DNA demethylation: mechanism, function and beyond. *Nat. Rev. Genet*. **18**, 517–534 (2017).
35. Koh, K. P. et al. Tet1 and Tet2 regulate 5-hydroxymethylcytosine production and cell lineage specification in mouse embryonic stem cells. *Cell Stem Cell* **8**, 200–213 (2011).
36. Gao, Y. et al. Replacement of Oct4 by Tet1 during iPSC induction reveals an important role of DNA methylation and hydroxymethylation in reprogramming. *Cell Stem Cell* **12**, 453–469 (2013).
37. Yu, H. et al. Tet3 regulates synaptic transmission and homeostatic plasticity via DNA oxidation and repair. *Nat. Neurosci*. **18**, 836–843 (2015).
38. Weng, Y.-L. et al. An intrinsic epigenetic barrier for functional axon regeneration. *Neuron* **94**, 337–346.e6 (2017).
39. Guo, J. U., Su, Y., Zhong, C., Ming, G. L. & Song, H. Hydroxylation of 5-methylcytosine by TET1 promotes active DNA demethylation in the adult brain. *Cell* **145**, 423–434 (2011).
40. Krishnan, A. et al. Overexpression of soluble Fas ligand following adeno-associated virus gene therapy prevents retinal ganglion cell death in chronic and acute murine models of glaucoma. *J. Immunol*. **197**, 4626–4638 (2016).
41. Almasieh, M. & Levin, L. A. Neuroprotection in glaucoma: animal models and clinical trials. *Ann. Rev. Vis. Sci*. **3**, 1–30 (2016).
42. Levin, L. A. et al. Neuroprotection for glaucoma: requirements for clinical translation. *Exp. Eye Res*. **157**, 34–37 (2017).
43. McClellan, A. J. et al. Ocular surface disease and dacryoadenitis in aging C57BL/6 mice. *Am. J. Pathol*. **184**, 631–643 (2014).
44. Li, H. et al. Single-cell transcriptomes reveal diverse regulatory strategies for olfactory receptor expression and axon targeting. *Curr. Biol*. **30**, 1189–1198.e5 (2020).
45. Mackay, D. S., Bennett, T. M. & Shiels, A. Exome sequencing identifies a missense variant in EFEMP1 co-segregating in a family with autosomal dominant primary open-angle glaucoma. *PLoS ONE* **10**, e0132529 (2015).
46. Marmorstein, L. Y. et al. Aberrant accumulation of EFEMP1 underlies drusen formation in Malattia Leventinese and age-related macular degeneration. *Proc. Natl Acad. Sci. USA* **99**, 13067–13072 (2002).
47. Wu, X., Li, G. & Xie, R. Decoding the role of TET family dioxygenases in lineage specification. *Epigenetics Chromatin* **11**, 58 (2018).
48. Neri, F. et al. Genome-wide analysis identifies a functional association of Tet1 and Polycomb repressive complex 2 in mouse embryonic stem cells. *Genome Biol*. **14**, R91 (2013).
49. Margueron, R. & Reinberg, D. The Polycomb complex PRC2 and its mark in life. *Nature* **469**, 343–349 (2011).
50. Mozhui, K. & Pandey, A. K. Conserved effect of aging on DNA methylation and association with EZH2 polycomb protein in mice and humans. *Mech. Ageing Dev*. **162**, 27–37 (2017).

Methods

No statistical methods were used to predetermine sample size. The mice were randomly assigned to experimental groups, except in experiments that required specific genotypes. The investigators were blinded to animal allocation but not cell cultures or outcome assessment.

Mouse lines

For optic-nerve crush and glaucoma model experiments, C57BL6/J wild type mice were purchased from the Jackson Laboratory (000664). Young and old females from the NIA Aged Rodent Colonies were used for ageing experiments. Rosa26-M2rtTA/Col1a1-tetOP-OKS-mCherry alleles were from the Hochedlinger laboratory (Massachusetts General Hospital)[51]. Rosa-CAG-lox-STOP-lox-Tomato mice were provided by F. Wang (McGovern Institute). Vglut2-IRES-Cre (016963), Vgat-IRES-Cre (016962), *Tet2*$^{flox/flox}$ (017573)[52] and Rosa26-M2rtTA/Col1a1-tetOP-OSKM (011011) were purchased from the Jackson Laboratory. All animal work was approved by the Institutional Animal Care and Use Committees (IACUCs) at Harvard Medical School, Boston Children's Hospital, and the Mass Eye and Ear Institution. Animals were housed under 12-h light/dark cycles (6:00/18:00), at an ambient temperature of 70–72 °F (21–22 °C) and 40–50% humidity.

Surgery

Mice were anaesthetized by intraperitoneal injection of a mixture of ketamine (100 mg kg^{-1}; Ketaset; Fort Dodge Animal Health) and xylazine (10 mg kg^{-1}; TranquiVed; Vedco) supplemented by topical application of proparacaine to the ocular surface (0.5%; Bausch & Lomb). All animal procedures were approved by the IACUC of the respective institutions and according to appropriate animal welfare regulations.

Production of adeno-associated viruses

Vectors of AAV-TRE-OSK were made by cloning mouse *Oct4*, *Sox2* and *Klf4* cDNA into an AAV plasmid consisting of the tetracycline response element (TRE3G) promoter and the SV40 element. The other home-made vectors were made using a similar strategy or directly chemically synthesized. All pAAVs, as listed (Supplementary Table 4), were then packaged into AAVs of serotype 2/2, 2/DJ or 2/9 (titres: >5 × 10^{12} genome copies per ml). AAVs were produced by the Boston Children's Hospital Viral Core.

Systemic delivery of AAV9

Expression in internal organs was achieved through retro-orbital injection of AAV9: 7 × 10^{11} gene copies (gc) of UBC-rtTA and 3 × 10^{11} gc of TRE-OSK for 5-month-old mice; 7 × 10^{11} gc of UBC-rtTA and 5 × 10^{11} gc of TRE-OSK (or TRE-GFP) for 20-month-old mice. To induce OSK expression, DOX (1 mg ml^{-1}; MP Biochemicals) was given in drinking water continuously until the end of the experiment, 3 weeks after AAV injection.

Cell culture of ear fibroblasts

Ear fibroblasts were isolated from Reprogramming 4F (Jackson Laboratory 011011) or 3F (Hochedlinger laboratory, Massachusetts General Hospital) mice and cultured at 37 °C in DMEM (Invitrogen) containing non-essential amino acids, 10% tetracycline-free fetal bovine serum (TaKaRa Bio, 631106) and 1% penicillin/streptomycin (ThermoFisher Scientific, 15140122). Ear fibroblasts of transgenic mice were passaged to P3 and treated with DOX (2 μg ml^{-1}) for the indicated time periods in the culture medium. All cell lines used were mycoplasma negative.

AAV2 intravitreal injection

Adult animals were anaesthetized with ketamine/xylazine (100/10 mg kg^{-1}), and then AAV (1–2 μl) was injected intravitreally, just posterior to the limbus with a fine glass pipette attached to a Hamilton syringe using plastic tubing. In the increased IOP model, mice received a 1 μl intravitreal injection between 3 and 4 weeks after microbead injection. The injected volume of AAV-shRNA is one-fifth the volume of other AAVs.

Optical coherence tomography

Optical coherence tomography (OCT) images were taken with a Bioptigen Envisu R-Class OCT (Leica Microsystems). The animals were anaesthetized with a ketamine/xylazine (100-200/20 mg kg^{-1}) cocktail and eyes were treated with a drop of 1% tropicamide solution to dilate the pupils and a drop of GenTeal gel to keep the lens hydrated. Full retinal OCT scans were obtained for all eyes (1,000×, 100×, 10). One-hundred B-scans were converted into videos (7 frames per second (fps)) with ImageJ. Representative OCT images of the retina were taken near the head of the optic nerve, and the imaging location was marked on the volume intensity projection image with a white line. The retinal thickness in each eye was measured using 4 B-scans at a distance of 50–600 μm on both sides of the optic nerve head and averaged using ImageJ.

Creation of retinoblastoma tumours

To create the space to inject the retinoblastoma tumour cells into the subretinal space, a transient retinal detachment was created. Intraocular pressure was decreased by first making a corneal incision, followed by a subretinal injection of 10,000 retinoblastoma tumour cells (Rb116) via a 30-gauge needle in a total volume of 10 μl. Two weeks after injection the mice were observed using OCT.

Optic nerve crush

Two weeks after intravitreal AAV injection, the optic nerve was accessed intraorbitally and crushed in anaesthetized animals using a pair of Dumont #5 forceps (FST). Alexa-conjugated cholera toxin beta subunit (CTB-555, 1 mg ml^{-1}; 1–2 μl) injection was performed 2 days before euthanasia to trace regenerating RGC axons. The surgical methods have been described in more detail previously[29].

In vivo DOX induction or suppression

Induction of the Tet-On or suppression of the Tet-Off AAV2 systems in the retina was performed by administration of DOX (2 mg ml^{-1}) (Sigma) in the drinking water. Induction of Tet-On AAV9 system systemically was performed by administration of DOX (1 mg ml^{-1}) (USP grade, MP Biomedicals 0219895505) in the drinking water.

Quantification of axon regeneration for the optic-nerve crush model

The number of regenerating axons in the optic nerve was estimated by counting the number of CTB-labelled axons at different distances from the crush site, as described previously[29].

Wholemount optic nerve preparation

Optic nerves and the connecting chiasm were dehydrated in methanol for 5 min, then incubated overnight with Visikol HISTO-1. The next day, nerves were transferred to Visikol HISTO-2 and then incubated for 3 h. Finally, optic nerves and connecting chiasm were mounted with Visikol HISTO-2.

Immunofluorescence

Wholemount retinas were blocked with horse serum at 4 °C overnight then incubated at 4 °C for 3 days with primary antibodies diluted in PBS, BSA (3%) Triton X-100 (0.5%). Then, tissues were incubated at 4 °C overnight with appropriate Alexa Fluor-conjugated secondary antibodies (Alexa 405, 488, 567, 674; Invitrogen) diluted with the same blocking solution as the primary antibodies, generally used at 1:400 final dilution. Frozen sections were stained overnight with primary antibodies at 4 °C and then secondary antibodies at room temperature for 2 h. Between changes of solutions, all wholemounts or slices were washed 3 times, for 5 min each time. Sections or wholemount

retinas were mounted with Vectashield Antifade Mounting Medium. Antibodies used were as follows: mouse anti-OCT4 (1:100, BD Bioscience 611203), rabbit anti-SOX2 (1:100, Cell Signaling 14962), goat anti-KLF4 (1:100, R&D systems AF3158), tabbit anti-phosphorylated S6 Ser235/236 (1:100, Cell Signaling 4857), mouse anti-BRN3A (1:200, EMD Millipore MAB1585), rabbit anti-Ki67(1:100, Abcam ab15580), mouse anti-AP2 alpha (1:100, Developmental Studies Hybridoma Bank 3B5), rabbit anti-pSTAT3 (Tyr705) (1:100, Cell Signaling 9145S), rat anti-HA (1:400, Roche 11867423001), rabbit anti-5mC (1:100, Cell Signaling 28692S), rabbit anti-5hmC (1:100, Active Motif 39769), rat anti-BrdU (1:200, Abcam ab6326), rabbit anti-Olig2 (1:100, Novusbio NBP1-28667), chicken anti-GFP (1:10,000, Aves Labs GFP-1020) and guinea pig anti-RBPMS (1:400, Raygene custom order A008712 to peptide GGKAEKENTPSEANLQEEEVRC). Note that successful staining for anti-5mC, anti-5hmC, anti-Ki67 and anti-BrdU requires pre-treatment with 2 M HCl for 30 min at room temperature, followed by 3 washes with 0.1 M sodium borate (pH 8.3) and PBST each before the serum blocking.

Bromodeoxyuridine labelling

After crush injury, mice were injected intraperitoneally with 5-bromo-2′-deoxyuridine (BrdU) (Sigma, B5002) at a dose of 100 mg kg^{-1} daily the week before they were euthanized. Optic nerves and retinas were collected either 1 or 2 wpc. Optic nerve sections and retina wholemounts were then performed with the same procedure described for immunofluorescence (including HCl pre-treatment) to complete the staining.

Western blot

SDS–PAGE and western blot analysis was performed according to standard procedures and detected with an ECL detection kit. Antibodies used: rabbit anti-SOX2 (1:100, EMD Millipore, AB5603), mouse anti-KLF4 (1:1,000, ReproCell, 09-0021), rabbit anti-p-S6 (S240/244) (1:1,000, CST, 2215), mouse anti-S6 (1:1,000, CST, 2317), mouse anti-β-tubulin (1:1,000, Sigma-Aldrich, 05-661), mouse anti-β-actin–Peroxidase antibody (1:20,000, Sigma-Aldrich, A3854).

RGC survival and phospho-S6 signal

RBPMS-positive cells in the ganglion layer were stained with an anti-RBPMS antibody (1:400, Raygene custom order A008712 to peptide GGKAEKENTPSEANLQEEEVRC), and a total of four 10× fields per retina, one in each quadrant, were enumerated. The average number of viable RGCs per field was determined. Phospho-S6 (1:100, Cell Signaling 4857) staining was performed under the same conditions and the percentages of phopsho-S6-positive RGCs were obtained by comparing the value to the number of all viable RGCs in the same field.

Human neuron differentiation and regeneration assay

We chose to use differentiated human neurons that would maintain ageing signatures[53]. SH-SY5Y neuroblastoma cells were obtained from the American Type Culture Collection (ATCC, CRL-2266). Cells were confirmed as negative for mycoplasma, then cultured in a 1:1 mixture of EMEM (ATCC, 30-2003) and F12 medium (Thermo Fisher Scientific, 11765054) supplemented with 10% FBS (Sigma, F0926) and 1% penicillin/streptomycin (Thermo Fisher Scientific, 15140122). Cells were cultured at 37 °C with 5% CO_2 and 3% O_2. Cells were passaged at around 80% confluency. SH-SY5Y cells were differentiated into neurons as previously described[54] with modifications. In brief, 1 day after plating, cell differentiation was induced for 3 days using EMEM/F12 medium (1:1) containing 2.5% FBS, 1× penicillin/streptomycin, and 10 μM all-*trans* retinoic acid (ATRA, StemCell Technologies, 72264) (Differentiation Medium 1), followed by a 3 day incubation in EMEM/F12 (1:1) containing 1% FBS, 1× penicillin/streptomycin, and 10 μM ATRA (Differentiation Medium 2). Cells were then split into 35-mm cell culture plates coated with poly-D-lysine (Thermo Fisher Scientific, A3890401). A day after splitting, neurons were matured in serum-free neurobasal/B27 plus culture medium (Thermo Fisher Scientific, A3653401) containing 1× Glutamax (Thermo Fisher Scientific, 35050061), 1× penicillin/streptomycin, and 50 ng ml^{-1} BDNF (Alomone Labs) (Differentiation Medium 3) for at least 5 days. Differentiated SH-SY5Y cells were transduced with AAV.DJ vectors at 10^6 genome copies per cell. Five days after transduction, vincristine (100 nM; Sigma, V8879) was added for 24 h to induce neurite degeneration. Neurons were then washed once with PBS and fresh Differentiation Medium 3 was added back to the plates. Neurite outgrowth was monitored for 2–3 weeks by taking phase-contrast images at 100× magnification every 3–4 days. Neurite area, axon number and length of each cluster of neurons were quantified using Image J.

Cell cycle analysis

Cells were collected and fixed with 70% cold ethanol for 16 h at 4 °C. After fixation, cells were washed twice with PBS and incubated with PBS containing 50 μg ml^{-1} propidium iodide (PI) (Biotium, 40017) and 100 μg ml^{-1} RNase A (Omega) for 1 h at room temperature. PI-stained samples were analysed on a BD LSR II analyser and only single cells were gated for analysis. Cell cycle profiles were analysed using FCS Express 6 (De Novo Software).

Human neuron DNA methylation analyses

DNA was extracted using the Zymo Quick DNA mini-prep plus kit (D4069) and DNA methylation levels were measured on Illumina 850 EPIC arrays. The Illumina BeadChip (EPIC) measured bisulfite-conversion-based, single-CpG resolution DNA methylation levels at different CpG sites in the human genome. Data were generated via the standard protocol of Illumina methylation assays (GSE147436), which quantifies methylation levels by the β value using the ratio of intensities between methylated and unmethylated alleles. Specifically, the β value was calculated from the intensity of the methylated (M corresponding to signal A) and unmethylated (U corresponding to signal B) alleles, as the ratio of fluorescent signals $\beta = \mathrm{Max}(M,0)/(\mathrm{Max}(M,0) + \mathrm{Max}(U,0) + 100)$. Thus, β values ranged from 0 (completely unmethylated) to 1 (completely methylated). 'Noob' normalization was implemented using the 'minfi' R package[55,56]. The mathematical algorithm and available software underlying the skin and blood clock for in vitro studies (based on 391 CpGs) has been previously published[57].

Microbead-induced increased intraocular pressure (IOP)

Increase of IOP was induced unilaterally by injection of polystyrene microbeads (FluoSpheres, Invitrogen; 15-μm diameter) to the anterior chamber of the right eye of each mouse under a surgical microscope, as previously reported[40]. In brief, microbeads were prepared at a concentration of 5.0×10^6 beads per ml in sterile physiologic saline. A 2-μl volume was injected into the anterior chamber through a trans-corneal incision using a sharp glass micropipette connected to a Hamilton syringe (World Precision Instruments) followed by an air bubble to prevent leakage. Any mice that developed signs of inflammation (clouding or an oedematous cornea) were excluded.

IOP measurements

IOPs were measured with a rebound TonoLab tonometer (Colonial Medical Supply) as previously described[40]. Mice were anaesthetized by 3% isoflurane in 100% oxygen (induction) followed by 1.5% isoflurane in 100% oxygen (maintenance) delivered with a precision vaporizer. IOP measurement was initiated within 2–3 min after the loss of a toe or tail pinch reflex. Anaesthetized mice were placed on a platform, and the tip of the pressure sensor was placed approximately 1/8 of an inch from the central cornea. Average IOP was displayed automatically after 6 measurements after elimination of the highest and lowest values. The machine-generated mean was considered as one reading, and six readings were obtained for each eye. All IOPs were taken at the same time of day (between 10:00 and 12:00) owing to the variation of IOP throughout the day.

Optomotor response

The visual acuity of mice was measured using an optomotor reflex-based spatial frequency threshold test[58]. Mice were able to freely move and were placed on a pedestal located in the centre of an area formed by four computer monitors arranged in a quadrangle. The monitors displayed a moving vertical black and white sinusoidal grating pattern. A blinded observer, unable to see the direction of the moving bars, monitored the tracking behaviour of the mouse. Tracking was considered positive when there was a movement of the head (motor response) to the direction of the bars or rotation of the body in the direction concordant with the stimulus. Each eye was tested separately depending on the direction of rotation of the grating. The staircase method was used to determine the spatial frequency start from 0.15 to 0.40 cycles per degree, with intervals of 0.05 cycles per degree. Rotation speed (12° s^{-1}) and contrast (100%) were kept constant. Responses were measured before and after treatment by individuals blinded to the group of the mouse and the treatment. Mice that had intravitreal bleeding or developed signs of inflammation (clouding or an oedematous cornea) during or post intravitreal injection were excluded from optomotor response and histological analyses. Exclusion criteria were pre-determined before experimentation.

Pattern electroretinogram

Mice were anaesthetized with ketamine/xylazine (100 mg kg^{-1} and 20 mg kg^{-1}) and the pupils dilated with one drop of 1% tropicamide ophthalmic solution. The mice were kept under dim red light throughout the procedure on a built-in warming plate (Celeris, Full-Field and Pattern Stimulation for the rodent model) to maintain their body temperature at 37 °C. A black and white reversing checkerboard pattern with a check size of 1° was displayed on light guide electrode-stimulators placed directly on the ocular surface of both eyes and centred with the pupil. The visual stimuli were presented at 98% contrast and constant mean luminance of 50 cd m^{-2}, with a spatial frequency of 0.05 cycles per degree and a temporal frequency of 1 Hz. A total of 300 complete contrast reversals of PERG were repeated twice in each eye and the 600 cycles were segmented, averaged and recorded. The averaged PERGs were analysed to evaluate the peak-to-trough N1 to P1 (positive wave) amplitude.

Quantification of optic-nerve axons in the glaucoma model

For quantification of axons, optic nerves were dissected and fixed overnight in Karnovsky's reagent (50% in phosphate buffer). Semi-thin cross-sections of the nerve were taken at 1.0 mm posterior to the globe and stained with 1% *p*-phenylenediamine (PPD) for evaluation by light microscopy. Optic-nerve cross-sections were imaged at 60× magnification using a Nikon microscope (Eclipse E800, Nikon) with DP Controller v.1.2.1.108 and DP Manager v.1.2.1.107 software (Olympus). Six to eight non-overlapping photomicrographs were taken to cover the entire area of each optic nerve cross-section. Using ImageJ (v.2.0.0-rc-65/1.51u), a 100 µm × 100 µm square was placed on each 60× image and all axons within the square (0.01 mm^2) were counted using the 'threshold' and 'analyze particles' functions in ImageJ as previously described[40,58,59]. Damaged axons stain darkly with PPD and were not counted. The average axon counts in the 6–8 images were used to calculate the axon density per mm^2 of optic nerve. Individuals performing axon counts were blinded to the experimental groups.

Quantification of retinal ganglion cells in the glaucoma model

For ganglion cell counting, images of wholemount retinas were acquired using a 63× oil immersion objective of the Leica TCS SP5 confocal microscope (Leica Microsystems). The retinal wholemount was divided into four quadrants and two to four images (248.53 µm × 248.53 µm in size) were taken from the midperipheral and peripheral regions of each quadrant, for a total of 12 to 16 images per retina. The images were obtained as *z*-stacks (0.5 µm), and all BRN3A-positive cells in the ganglion cell layer of each image were counted using an automated counting platform as previously described[59,60]. In brief, RGCs were counted using the 'Cell Counter' plugin (http://fiji.sc/Cell_Counter) in Fiji (ImageJ Fiji, v.2.0.0-rc-69/1.52n). Each image was loaded into Fiji, and a colour counter type was chosen to mark all BRN3A-stained RGCs within each image (0.025 mm^2). The average number of RGCs in the 12–16 images were used to calculate the RGC density per square millimetre of retina. Two individuals blinded to the experimental groups performed all RGC counts.

RGC enrichment

Retinas were dissected in AMES solution (oxygenated with 95% O_2/5% CO_2), digested in papain, and dissociated to single-cell suspensions with manual trituration in ovomucoid solution. Cells were spun down at 450*g* for 8 min, and resuspended in AMES + 4%BSA to a concentration of 10^5 cells per ml. Thy1.2-PE-Cy7 antibody (1:2,000, Invitrogen 25-0902-81) was added and incubated for 15 min, followed by washing with an excess of media. Cells were spun down at 450*g* for 8 min and resuspended again in AMES + 4%BSA at a concentration of around 7×10^6 cells per ml. The live cell marker Calcein Blue (1 µl ml^{-1}) was added before filtering cells through 35-µm cell strainer into fluorescence activated cell sorting (FACS) tubes. More than 10,000 high Thy1.2+ and Calcein Blue+ cells were collected using a BD FACS Aria Cell Sorter with an 130-µm nozzle. Frozen cells were sent to Genewiz for RNA extraction and ultra-low input RNA sequencing, or to Zymo Research for DNA extraction and genome-wide reduced representation bisulfite sequencing (RRBS).

RRBS library preparation

RGC DNA from mice at different ages and treatments (Supplementary Table 5) was extracted using Quick-DNA Plus Kit Microprep Kit. Starting input genomic DNA (2–10 ng) was digested with 30 units of MspI (NEB). Fragments were ligated to pre-annealed adapters containing 5′-methylcytosine instead of cytosine according to Illumina's specified guidelines. Adaptor-ligated fragments ≥50 bp in size were recovered using the DNA Clean & Concentrator-5 (cat. no.: D4003). The fragments were then bisulfite-treated using the EZ DNA Methylation-Lightning Kit (cat. no.: D5030). Preparative-scale PCR products were purified with DNA Clean & Concentrator-5 (cat. no.: D4003) for sequencing on an Illumina HiSeq using 2 × 125 bp paired end (PE).

DNA methylation analysis of mouse RGC

Reads were filtered using Trim Galore v.0.4.1 and mapped to the mouse genome GRCm38 using Bismark v.0.15.0. Methylation counts on both positions of each CpG site were combined. Only CpG sites covered in all samples were considered for analysis (BioProject, PRJNA655981). Two outliers were excluded by low intercorrelation (<0.93) within the batch (Supplementary Table 5). This resulted in a total of 703,583 sites covered by uniquely mapped reads. Differential methylation for each CpG site was calculated using two-tailed Student's *t*-tests on every site independently, followed by the Benjamini–Hochberg procedure to adjust for false discovery rate. The delta value between groups was calculated as the difference between the means of values in two corresponding groups of samples. Gene Ontology analysis of differentially methylated sites was performed with Cistrome-GO (http://go.cistrome.org). Owing to the repetitive nature of ribosomal DNA sequence, it is not suitable for whole genome bisulfite mapping. Thus, to determine the ribosomal DNA methylation age, reads were mapped to ribosomal DNA repeat BK000964 and the coordinates were adjusted accordingly[33]. 67 out of 72 sites with at least 10 reads per site were covered for the ribosomal DNA methylation clock, compared to 102/435 sites of the whole lifespan multi-tissue clock[61], or 248/582 and 77,342/193,651 sites (ridge) of two entire lifespan multi-tissue clocks[62]. In agreement with previous studies[57,63,64], estimates of the DNA methylation age of neurons tend to be lower than their chronological age but remain correlated.

DNA methylation ageing signature

Sorted RGC samples were split into training and test sets, with $n = 38$ samples used for candidate CpG selection and biomarker construction and $n = 23$ samples used for validation (Supplementary Table 6, Supplementary Data and code within the Supplementary Information). The training samples included those from 1-month-old controls (1 mo; $n = 6$), 6-month-old ($n = 8$), 12-month-old ($n = 2$), 18-month-old ($n = 8$), 30-month-old ($n = 6$), 1-month-old GFP-injured ($n = 4$), 12-month-old GFP ($n = 2$) and 12-month-old OSK ($n = 2$) mice. To generate a methylation ageing signature, we evaluated DNA methylation associations with three traits: age, injury and OSK treatment. To avoid batch effects, subsamples were evaluated separately as 6-month-old and 18-month-old in Batch 1, and 1-month-old, 12-month-old and 30-month-old in Batch 2 (Supplementary Table 5). Biweight midcorrelation was used to assess age trends for CpGs. Given that the second batch included samples from developing (1-month-old) mice, we applied a transformation to age that has been used in development of human epigenetic clocks when prenatal and/or developmental samples are included[4]. This transformation accounts for nonlinear changes during development. Biweight midcorrelation was then applied to test the associations of CpGs changes after injury and OSK treatment, and results were compared across the four tests. CpGs were selected if they were consistently in the top 30% of CpGs with the strongest absolute biweight midcorrelations in all four tests and showed consistency in the directionality of their associations (for example, hypomethylated with age in both batches, hypomethylated with injury, and hypermethylated after OSK). Of the 703,583 CpGs that were considered, 1,226 were selected (723 that trended towards hypermethylation with age and 503 that trended towards hypomethylation with age, see Supplementary Table 3). Principal component analysis (PCA) was conducted using the training samples from 1-month-old, 12-month-old and 30-month-old controls ($n = 14$). PC1 explained 25% of the variance in this sample. When applying an elastic net model to train a predictor of age, PCs beyond PC1 did not increase the robustness of the age prediction[65]. Thus, PC1 was used to represent the ageing signature and was standardized to have a mean = 0 and s.d. = 1. Analyses of the ageing signature in independent validation samples were then conducted to test associations with age, injury and OSK.

Transcription-factor binding and histone modification enrichment

To identify factors that may mediate epigenetic reprogramming in RGCs, we performed transcription factor (TF) binding enrichment and histone modification enrichment analyses using the genome coordinates (GRCm38/mm10) of the 1,226 selected CpGs using the CistromeDB Toolkit (http://dbtoolkit.cistrome.org). A sensitivity analysis was conducted by performing TF and histone enrichment for five sets of 1,226 random CpGs from the 702,357 unselected sites, which was then compared against the enrichment for our selected set in order to identify TFs and histone marks that were specific to the selected set but not to CpGs in general.

Total RNA extraction and sample quality control

Total RNA was extracted following the TRIzol Reagent User Guide (Thermo Fisher Scientific). Glycogen (1 µl of 10 mg ml^{-1} solution) was added to the supernatant to increase RNA recovery. RNA was quantified using a Qubit 2.0 Fluorometer (Life Technologies), and RNA integrity was determined using TapeStation (Agilent Technologies).

Ultra-low-input RNA library preparation and multiplexing

RNA samples were quantified using a Qubit 2.0 Fluorometer (Life Technologies), and RNA integrity was ascertained using a 2100 TapeStation (Agilent Technologies). RNA library preparations, sequencing reactions, and initial bioinformatics analysis were conducted at Genewiz. A SMART-Seq v4 Ultra Low Input Kit for Sequencing was used for full-length cDNA synthesis and amplification (Clontech), and Illumina Nextera XT library was used for sequencing library preparation. In brief, cDNA was fragmented and adaptors were added using Transposase, followed by limited-cycle PCR to enrich and add an index to the cDNA fragments. The final library was assessed by a Qubit 2.0 Fluorometer and an Agilent TapeStation.

Paired-end sequencing

The sequencing libraries were multiplexed and clustered on two lanes of a flowcell. After clustering, the flowcell was loaded on the Illumina HiSeq instrument according to the manufacturer's instructions. Samples were sequenced using a 2 × 150 paired-end configuration. Image analysis and base calling were conducted by the HiSeq Control Software on the HiSeq instrument. Raw sequence data (.bcl files) generated from an Illumina HiSeq was converted into fastq files and de-multiplexed using the Illumina bcl2fastq v.2.17 program. One mismatch was allowed for index sequence identification.

RNA sequencing analysis

Paired-end reads were aligned with hisat2 v.2.1.0[66] to the Ensembl GRCm38 primary assembly using splice junctions from the Ensembl release 84 annotation. Paired read counts were quantified using featureCounts v.1.6.4[67] using reads with a mapping quality (mapQ) value ≥ 20. Differentially-expressed genes for each pairwise comparison were identified with edgeR v.3.26[68], testing only genes with at least 0.1 counts per million (CPM) in at least three samples. Gene Ontology analysis of differentially expressed genes (BioProject PRJNA655981) was performed with AmiGO v.2.5.12[69–71]. The gene selection criteria for the experiments in Fig. 4c, 4d and Extended Data Fig. 9i, 9j are as follows: genes significantly changed during ageing ($q < 0.05$, absolute $\log_2$ fold-change > 1), not low expressed ($\log_2$(CPM) > −2) or altered by mock AAV infection (old vs old (−OSK), $q > 0.1$).

Statistical analysis and figure preparation

Statistical analyses were performed with GraphPad Prism 7/8, using two-tailed Student's *t*-tests, one-way or two-way ANOVA. All of the statistical tests performed are indicated in the figure legends. The data are presented as mean ± s.e.m., except for the violin plots in Extended Data Fig. 8e, f, which show median and quartiles. Statistical analysis of changes to DNA methylations was performed with the SciPy package in Python. Figures were prepared using Keynote and Affinity Designer.

Reporting summary

Further information on research design is available in the Nature Research Reporting Summary linked to this paper.

Data availability

RRBS data for DNA methylation analysis and RNA sequencing data are available in the BioSample database (NCBI) and under BioProject PRJNA655981. Illumina Human Methylation EPIC array data are available in the Gene Expression Omnibus (GEO) database (NCBI) and under GSE147436. All other relevant data that support the findings of this study are available from the corresponding author upon reasonable request. Source data are provided with this paper.

Code availability

The code for determining methylation ageing signatures is provided in the Supplementary Information.

51. Bar-Nur, O. et al. Small molecules facilitate rapid and synchronous iPSC generation. *Nat. Methods* **11**, 1170–1176 (2014).
52. Moran-Crusio, K. et al. Tet2 loss leads to increased hematopoietic stem cell self-renewal and myeloid transformation. *Cancer Cell* **20**, 11–24 (2011).

53. Mertens, J. et al. Directly reprogrammed human neurons retain aging-associated transcriptomic signatures and reveal age-related nucleocytoplasmic defects. *Cell Stem Cell* **17**, 705–718 (2015).
54. Shipley, M. M., Mangold, C. A. & Szpara, M. L. Differentiation of the SH-SY5Y human neuroblastoma cell line. *J. Vis. Exp.* **108**, e53193 (2016).
55. Triche, T. J., Jr, Weisenberger, D. J., Van Den Berg, D., Laird, P. W. & Siegmund, K. D. Low-level processing of Illumina Infinium DNA Methylation BeadArrays. *Nucleic Acids Res.* **41**, e90 (2013).
56. Fortin, J. P., Triche, T. J., Jr & Hansen, K. D. Preprocessing, normalization and integration of the Illumina HumanMethylationEPIC array with minfi. *Bioinformatics* **33**, 558–560 (2017).
57. Horvath, S. et al. Epigenetic clock for skin and blood cells applied to Hutchinson Gilford Progeria Syndrome and *ex vivo* studies. *Aging (Albany NY)* **10**, 1758–1775 (2018).
58. Sun, D., Moore, S. & Jakobs, T. C. Optic nerve astrocyte reactivity protects function in experimental glaucoma and other nerve injuries. *J. Exp. Med.* **214**, 1411-1430 (2017).
59. Krishnan, A., Kocab, A. J., Zacks, D. N., Marshak-Rothstein, A. & Gregory-Ksander, M. A small peptide antagonist of the Fas receptor inhibits neuroinflammation and prevents axon degeneration and retinal ganglion cell death in an inducible mouse model of glaucoma. *J. Neuroinflammation* **16**, 184 (2019).
60. Dordea, A. C. et al. An open-source computational tool to automatically quantify immunolabeled retinal ganglion cells. *Exp. Eye Res.* **147**, 1218–1235 (2013).
61. Meer, M. V., Podolskiy, D. I., Tyshkovskiy, A. & Gladyshev, V. N. A whole lifespan mouse multi-tissue DNA methylation clock. *eLife* **7**, e40675 (2018).
62. Thompson, M. J. et al. A multi-tissue full lifespan epigenetic clock for mice. *Aging (Albany NY)* **10**, 2832–2854 (2018).
63. Horvath, S. et al. The cerebellum ages slowly according to the epigenetic clock. *Aging (Albany NY)* **7**, 294–306 (2015).
64. Hoshino, A., Horvath, S., Sridhar, A., Chitsazan, A. & Reh, T. A. Synchrony and asynchrony between an epigenetic clock and developmental timing. *Sci. Rep.* **9**, 3770 (2019).
65. Levine, M. et al. A rat epigenetic clock recapitulates phenotypic aging and co-localizes with heterochromatin. *eLife* **9**, e59201 (2020).
66. Kim, D., Langmead, B. & Salzberg, S. L. HISAT: a fast spliced aligner with low memory requirements. *Nat. Methods* **12**, 357–360 (2015).
67. Liao, Y., Smyth, G. K. & Shi, W. featureCounts: an efficient general purpose program for assigning sequence reads to genomic features. *Bioinformatics* **30**, 923–930 (2014).
68. Robinson, M. D., McCarthy, D. J. & Smyth, G. K. edgeR: a Bioconductor package for differential expression analysis of digital gene expression data. *Bioinformatics* **26**, 139–140 (2010).
69. Carbon, S. et al. AmiGO: online access to ontology and annotation data. *Bioinformatics* **25**, 288–289 (2009).
70. Ashburner, M. et al. Gene Ontology: tool for the unification of biology. *Nat. Genet.* **25**, 25–29 (2000).
71. The Gene Ontology Consortium. The Gene Ontology Resource: 20 years and still GOing strong. *Nucleic Acids Res.* **47**, D330–D338 (2019).

Acknowledgements We thank A. Wagers, R. Mostoslavsky, Y. Shi, A. Das, A. Pogoutse, C. Petty, A. Coffey, B. Zhang, P. Dmitriev, K. Booher, E. Chen, J. Wang, D. Vogel, M. Thompson, A. Jacobi and S. Hou for advice and assistance; and Y. Weng, H. Song and F. Wang for reagents and mice. The work was supported by the Harvard Medical School Epigenetics Seed Grant and Development Grant; The Paul F. Glenn Foundation for Medical Research; a gift from E. Schulak; NIH awards R01AG019719 and R37AG028730 (to D.A.S.), R01EY026939 and R01EY021526 (to Z.H.), R01AG067782 and R01GM065204 (to V.N.G.) and R01AG065403 (to M.E.L. and V.N.G.). We thank Boston Children's Hospital Viral Core, which is supported by NIH5P30EY012196; and Schepens Eye Institute Core facilities, supported by NEI-P30EY003790. X.T. was supported by NIH award K99AG068303 and by NASA Postdoctoral Fellowship 80NSSC19K0439; D.L.V. was supported by NIH training grant T32AG023480; J.-H.Y. was partially supported by National Research Foundation of Korea (2012R1A6A3A03040476); B.R.K. was partially supported by the St Vincent de Paul Foundation and by NEI awards R24EY028767 and R01EY025794; and M.S.G.-K. by NEI award R21EY030276. We thank P. F. Glenn for his mentorship and support of ageing research.

Author contributions Y.L. and D.A.S. conceived the project. Y.L., X.T. and D.A.S. wrote the manuscript with input from all co-authors. Y.L. was involved in all experiments and analyses. M.S.B. and J.-H.Y. provided early training to Y.L. B.B., C.W., Q.Z., D.Y., S.Z. and Z.H. contributed to the optic nerve crush studies and imaging. A.K., D.Y., Q.Z., E.M.H., E.K., M.S.G.-K. and B.R.K. contributed to the glaucoma and ageing studies. M.M.K. and B.R.K. performed OCT imaging and analysis. M.M. and V.N.G. conducted ribosomal DNA methylation age analysis for mouse RGCs. M.E.L. developed the DNA methylation ageing signature. D.L.V. performed the RNA sequencing and gene association analysis. X.T. conducted human neuron experiments. S.H. conducted the human methylation clock analysis. X.T., J.-H.Y. and K.H. helped with the work on transgenic mouse fibroblasts. M.S.B., X.T., M.B.S., A.E.K. and L.A.R. helped with systemic AAV9 experiments. N.D. and G.M.C. helped with plasmid constructs and AAV9 production. K.C. helped with grant applications and project management.

Competing interests D.A.S. is a consultant to, inventor of patents licensed to, board member of and equity owner of Iduna Therapeutics, a Life Biosciences company developing epigenetic reprograming therapies. D.A.S. is an advisor to Zymo Research, an epigenetics tools company. Additional disclosures are at https://genetics.med.harvard.edu/sinclair/people/sinclair-other.php. Y.L., L.A.R. and S.H. are equity owners of Iduna Therapeutics, a Life Biosciences company. D.L.V. is an advisor to Liberty Biosecurity. M.S.B. is a shareholder in MetroBiotech. K.C. is an equity owner in Life Biosciences and affiliates. N.D. and G.M.C. are co-founders of Rejuvenate Bio. Disclosures for G.M.C. can be found at http://arep.med.harvard.edu/gmc/tech.html. M.E.L. is a bioinformatics advisor to Elysium Health. Y.L., N.D. and D.A.S. are inventors on patents arising from this work (WO/2020/069373 and WO/2020/069339), filed by the President and Fellows of Harvard College. The other authors declare no competing interests.

Additional information

Supplementary information is available for this paper at https://doi.org/10.1038/s41586-020-2975-4.

Correspondence and requests for materials should be addressed to D.A.S.

Peer review information *Nature* thanks Andrew Huberman, Hongjun Song, Yasuhiro Yamada and the anonymous reviewer(s) for their contribution to the peer review of this work. Peer reviewer reports are available.